Joint Inversion of Receiver Functions and Apparent Incidence Angles to Determine the Crustal Structure of Mars

Rakshit Joshi, Brigitte Knapmeyer-Endrun, Klaus Mosegaard, M. Wieczorek, Heiner Igel, Ulrich Christensen, Philippe Lognonné

S1222a - the largest Marsquake detected by InSight

Taichi Kawamura[1], John F. Clinton[2], Géraldine Zenhäusern[3], Savas Ceylan[3], Anna C. Horleston[4], Nikolaj L. Dahmen[3], Cecilia Duran[3], Doyeon Kim[3], Matthieu Plasman[1], Simon C. Stähler[3], Fabian Euchner[3], Constantinos Charalambous[5], Domenico Giardini[3], Paul Davis[6], Grégory Sainton[1], Philippe Lognonné[1], Mark Panning[7], William B. Banerdt[7]

[1]Université Paris Cité, Institute de physique de globe de Paris, CNRS, Paris, France
[2]Swiss Seismological Service, ETH Zurich, Zurich, Switzerland
[3]Institute of Geophysics, ETH Zurich, Zurich, Switzerland
[4]School of Earth Sciences, University of Bristol, Bristol, UK
[5]Imperial College London, London, UK
[6]University of California, Los Angeles, USA
[7]Jet Propulsion Laboratory, Pasadena, USA

Key Points:

- InSight detected on May, 4, 2022 a $M_W^{Ma}4.7$ marsquake, S1222a, which is the largest seismic event detected so far.
- The exceptional signal-to-noise allows multiple phases to be identified, with a rich collection of surface waves.
- S1222a was located 37 degrees southeast of the InSight landing site and close to the Martian dichotomy boundary.

Corresponding author: Taichi Kawamura, `kawamura@ipgp.fr`

Abstract

NASA's InSight has detected a large magnitude seismic event, labelled S1222a. The event has a moment magnitude of M_W^{Ma}4.7, with 5 times more seismic moment release compared to the second largest even. The event is so large that features are clearly observed that were not seen in any previously detected events. In additional to body phases and Rayleigh waves, we also see Love waves, minor arc surface wave overtones, and multi-orbit surface waves. At long periods, the coda event exceeds 10 hours. The event locates close to the North-South dichotomy and outside the tectonically active Cerberus Fossae region. S1222a does not show any evident geological or tectonic features. The event is extremely rich in frequency content, extending from below 1/30 Hz up to 35 Hz. The event was classified as a broadband type event; we also observe coda decay and polarization similar to that of very high frequency type events.

1 Introduction

NASA's Interior Exploration using Seismic Investigations, Geodesy and Heat Transport (InSight) mission has achieved almost continuous seismic monitoring of Mars since early 2019 (Banerdt et al., 2020; Lognonné et al., 2020). Since May 2022, the local background seismic noise has increased due to the typical atmospheric disturbance observed during the Martian autumn and winter, and the power situation had deteriorated to the point that InSight's SEIS (Seismic Experiment for Interior Structure) instrument (Lognonné et al., 2019) was about to begin to be periodically switched off. In this challenging situation, SEIS recorded the largest marsquake ever detected during the mission lifetime to date. On May 4^{th}, at 23:23:07 UTC, also known as the 1222^{nd} Martian day (sol) since InSight landed, a magnitude M_W^{Ma}4.7 marsquake shook the red planet. The aim of this paper is to describe in detail the main characteristics of the event and provide initial context for further research.

To uncover the internal structure of Mars, InSight was equipped with a suite of geophysical instruments and seismic sensors; SEIS is one of the key scientific instruments of the mission (Banerdt et al., 2020; Lognonné et al., 2019; Lognonné et al., 2020). Since the deployment, SEIS has been monitoring Martian seismicity for more than 1350 sols (each sol is approximately 24h39m). SEIS consists of two seismometers, the Very Broadband (VBB) seismometer and the Short Period (SP) seismometer designed to cover the different frequency bands. InSight also has a series of environmental monitoring sensors known as the Auxiliary Payload Sensor Suite (APSS). APSS includes meteorological sensors (pressure, wind and thermal sensors) and a magnetometer (Banfield et al., 2019, 2020; Johnson et al., 2020). SEIS data are strongly contaminated by environmental, spacecraft and instrumental noise (Ceylan et al., 2021; Scholz et al., 2020; Kim, Davis, et al., 2021). In the nominal configuration, InSight simultaneously observes both seismic signals and environmental noise, which allows seismologists to distinguish between true seismic events and environmental noise injection (Clinton et al., 2021; Charalambous et al., 2021). However, this was no longer possible since Sol 789 due to power limitations that required shut down of some of the scientific payload. The two solar panels that are used to power the spacecraft and the instrument have steadily accumulating Martian dust and the power generation has degraded significantly. Thus, for the last 600 sols, SP and APSS were only occasionally powered on and only the VBB has been powered on continuously, with sampling at 20 Hz. Neither the SP nor APSS were turned on during S1222a. VBB was operating in high-sampling-rate mode and it was possible to also retrieve 100 Hz for the event. SEIS data is archived and released by InSight Mars SEIS Data Service and the data is available to the science community with 3 months delay (InSight Mars SEIS Data Service, 2019).

Using InSight seismic data, various Marian seismic velocity models were proposed (Giardini et al., 2020; Lognonné et al., 2020; Stähler et al., 2021; Khan et al., 2021; Knapmeyer-

Endrun et al., 2021; Kim, Lekić, et al., 2021; Drilleau et al., 2021, 2022). MQS uses the suite of models proposed in Stähler et al. (2021) to locate seismic events. This approach was proven to be highly plausible after the remarkable precision we achieved for detected impacts whose locations were confirmed using orbital imaging (Garcia et al., 2022; Posiolova et al., 2022). Back azimuths are obtained based on the method described in Zenhäusern et al. (2022). This method provides a more rigorous and systematic estimation of the polarization compared to the former approach described in Böse et al. (2017), not least since it combines observations from both P and S arrivals. Its efficacy was also demonstrated through analyses of ambient noise (Stutzmann et al., 2020). Event depths are challenging to define using only a single station where depth phases are rarely identified, so MQS assigns a fixed depth of 50 km to all events.

2 Event Overview

Figure 1 and Table 1 show the general characteristics of event S1222a and the context of the background environmental noise. Waves from the event first reached InSight shortly before 4AM Local Mean Solar Time (LMST) on Mars. S1222a occurred in mid-autumn at the landing site, a season with high seismic noise due to persistent winds. Broadband noise injection from wind was observed constantly before and during the event as evidenced by the presence of clear lander resonances (Dahmen et al., 2021; Charalambous et al., 2021). In addition to the environmental noise, InSight data suffers from glitches which are likely due to thermal-induced shocks within the instrument or the lander (Scholz et al., 2020). Glitches are 1-sided pulses that can be modelled by the instrument response to a step in acceleration, and hence appear as near-critically damped 20s signals, that are rich in all frequencies. The signals regularly corrupt the seismic signal and obscure phase interpretation (Kim, Davis, et al., 2021). Despite the very high amplitude seismic signals, strong glitches are present throughout S1222a. To avoid misinterpretation of seismic phases with glitches, analysis of the data is performed on both raw data as well as deglitched data following the methods described in Scholz et al. (2020).

Despite the high background noise, the seismic energy of the event strongly exceeds the noise level (Figure1(d)). The event is rich in frequency content and for many minutes following the energy onset, signal far exceeds the noise level from below 30 seconds to 35 Hz. Comparing the seismic spectra to the background noise, the signal to noise ratio is as high as 40 dB at ∼30 seconds and 60 dB at ∼1Hz (Figure1(d)). Following the MQS convention, since there is very significant energy below 2.4 Hz, the event is cataloged as a Broadband (BB). This event is remarkable in many ways - low-frequency energy persists for approximately 10 hours (Figure1(b)). While the high frequency energy above 1 Hz attenuates far more rapidly (∼20 min) than the long period, the resonance at 2.4 Hz continues to ring for an additional (∼20 min). Previously, no broadband event included energy above 10 Hz, yet in S1222a energy is clearly present up to 35 Hz and is strongest on the horizontal components at high frequencies - behaviour that otherwise is only observed in Very High Frequency (VF) events. The event spectrum is so broad and large it spans all previously known event types.

The peak amplitude of the signal reaches 2.8×10^{-5} m/s on the instrument-response-corrected radial components. On the oblique components of the raw data, the value is 2.4×10^{-5} m/s, equivalent to 2.2 millions counts. It is noted that this is 26% of the 2^{23}count limit of the 24-bit EBOX digitiser (Zweifel et al., 2021). SEIS was remarkably close to saturation during this event.

2.1 Phase Identification

Two energy packets can be clearly identified that are interpreted as P and S body waves, as has been done for other Low Frequency family events (Clinton et al., 2021; Ceylan et al., 2021)(Figure1(e)). The onset of each packet is picked as the first arrival of each

phase. The P coda has almost constant amplitude across the minutes before the S arrival. After the arrival of the stronger S phase, energy gradually decays which is a typical characteristic of the High Frequency family of marsquakes (Figure1(e)).

In addition to the routinely identified body phases, surface waves are clearly visible in the S-wave coda (Figure1(a,b,c)). To date, the only surface waves identified on Mars have been fundamental Rayleigh waves that were observed in 2 other events, S1000a and S1094b (Kim et al., 2022). In the case of S1222a, a much richer set of surface waves are observed. Both fundamental Rayleigh and Love waves (R1 and G1 respectively), and first overtones (R1_1 and G1_1), can be identified. Further, major arc R2 and multi orbit R3, although weak, can be identified, and there are suggestions of later multi-orbit arrivals (x4, x5). All the phase arrival picks that were made by MQS are summarized in Table 1. We will describe in detail in the following the phases that we identified.

2.1.1 Body Waves

The first clear arrival visible in the data is an impulsive P wave. The P arrival was picked in the time domain which is only possible for events with a high signal-to-noise ratio, such as 14 quality A events. 1.5-10 seconds filtered data were used to identify the downward motion of the P arrival with an uncertainty of 0.5 seconds. In Figure 2 we can see a clear impulsive and broadband P arrival between 3 Hz - 10 s, though above 3 Hz there is a distinct delay in arrival time that increases linearly with frequency, possibly the effect of scattering at higher frequencies. The P arrival is glitch free though a large glitch is observed within the P coda (obvious glitches are indicated in the timeseries shown in Figure 1(e,f)). Polarisation analysis (see below) shows that this phase is strongly and persistently polarised. A stronger second envelope of energy arrives approximately 3.5 min later, consistent with an S phase arrival. The polarisation is persistent and different to the P-wave, allowing us to label it as a S-phase (Figure3). The impulsive S arrival can also be identified in the time series, for the MQS phase pick we used data filtered between 1.5 and 10 seconds, and assigned a 2 seconds uncertainty. As in the case for P wave, the S wave also shows an impulsive broadband arrival though is similarly delayed at higher frequencies. A large number of significant glitches are present in the S-wave coda, though they are not clearly visible in the raw time series since the signal amplitudes are so high - they are revealed if the signal is integrated to displacement.

Both the P and S wave coda include high frequency energy that reaches up to $\sim$32.5 Hz with signal to noise ratio larger than 10(Figure 2). In order to be be consistent with other broadband events in the catalogue, MQS also identified y1 and y2 arrivals which correspond to the arrival times of the high frequency portion of the energy and are picked using the energy envelope at the 2.4Hz resonance (Ceylan et al., 2021). As expected, arrivals are very similar to the P and S arrivals, lying within the error bars, as shown in Table 1. As for other VF events, S1222a has stronger horizontal energy at high frequencies and the horizontal energy persists to higher frequencies while the vertical energy decays quickly (Figure 1(c),(d))(van Driel et al., 2021; Menina et al., 2021; Karakostas et al., 2021).

2.1.2 Surface Waves

Almost no other marsquake had energy above the noise below 10s. At periods from about 10-30 seconds, S1222a exhibits dispersive signals which are a strong indication of surface waves. Surface waves were first reported for two large impacts where the surface source efficiently excited surface waves (Kim et al., 2022). The polarised P-wave allows us to rotate the signal into radial and transverse components, aiding our interpretation. For S1222a, on the vertical and radial components, we see a clear Rayleigh wave between at least 10 and 35 seconds period, starting about 4.5 minutes after the S arrival (Figure**??**. As shown in Table 1 and visible in Figure1(c), the signal shows clear dispersion where

phase arrivals are delayed towards the high frequencies. Furthermore, we can also identify a first overtone arriving before the fundamental mode. The overtone is shifted towards the higher frequencies and the dispersive signal is detected in the period range of 3 - 15 seconds. As expected for the overtone, the two signals show similar dispersion. In addition to the Rayleigh wave, on the transverse component, a Love wave was detected for the first time on Mars for S1222a at 23:33:38.2, which is about 2 minutes after the S arrival. The Love wave arrives about 2.5 minutes before the Rayleigh wave and almost at the same time as the Rayleigh wave overtone.

2.2 Multi-orbit Surface Waves

S1222a not only enabled us to identify Love waves for the first time on Mars, it also provides us with opportunities to explore further subsequent surface waves. In Figure 1(a), where we plot a 12 hour spectrogram in acceleration, we see energy significantly higher that the background noise at 01:15(UTC). The signal shows a weak dispersion but this is difficult to confirm with the low signal to noise ratio. The energy is followed by another packet of energy about 20 minutes later. This signal is overlapping with a significant glitch but is clearly visible after the deglitching (Figure1(f)). These signals are only visible in the vertical component and this makes it difficult for us to investigate the polarization of these signals. However, given the dispersive feature of the signal, we concluded that these are the R2 and R3 phases and their picks are also provided in Table1. Similar multi-orbit phases were not identified for Love waves which is reasonable given the higher noise level on the horizontal components, where Love waves should be most visible. This is the first time that we have identified and catalogued R2 and R3.

2.3 Distance Analysis

As done throughout the mission, we used P and S arrivals and a suite of reference seismic velocity models (Stähler et al., 2021) to find the most probable location (modified after (Böse et al., 2017)). This provides a distance consistent with all the other events in the catalog (Ceylan et al., 2021) and we are confident that this gives us a reasonable distance after the detection of confirmed impacts (Posiolova et al., 2022). This gave us 37 degrees for the distance. We refrain from using fundamental and overtone surface wave arrival times here since our methods are not yet calibrated for these phases.

Our pre-landing plan was to use R1/2/3 to locate marsquakes with a single station. This method was described in various pre-landing papers but was not used to date given the lack of R2/R3 detection (Panning et al., 2015; Böse et al., 2017; van Driel et al., 2019). Given that this is our first detection of R2 and R3, we tested this method to locate the marsquake and compared with the distance obtained from the body waves. With R1/2/3, we obtained 35.4 degrees which is consistent and overlaps with the value obtained with body waves within the range of the errorbar. While S1222a enabled us to at last confirm our pre-landing concept, we did not include this as the preferred location for consistency with other events in the catalog.

2.4 Back-azimuth Analysis

Figure 3(a) shows the result of the back azimuth analysis for body waves by using the eigenvector method described in Zenhäusern et al. (2022) and adopted by MQS from catalog V12. Data here includes a linearity filter to accentuate body wave energy, which is defined as $F_e = (1 - \epsilon)^2$. ϵ is the ellipticity of the signal and is 0 for a rectilinear and 1 for a circular signal (for details see Zenhäusern et al. (2022)). The P energy observed between 1/10-1/2 Hz, the window MQS uses to determine LF family polarization, has a polarization that peaks at 101 degrees. This value is consistent over a wide frequency band, from 1/10 to 2 Hz and time window (shown in yellow in Figure 3(a)). As is normal for marsquakes, high frequency energy is intensely scattered. The incident

angles of about 70-80 degrees (shown in orange in the figure) are observed at 1/5-1/2 Hz. Such vertical polarization supports our identification of the P wave. When we focus on the S wave, we also see coherent energy around a similar frequency band as the P wave which clearly has a different back-azimuth of about 0°, about 90°shifted from the P polarization, and having a low inclination angle of about 20°. Both are consistent with an S-wave.

Figure 3(b) shows the same polarization analyses, but without linearity filter, in order to accentuate surface wave energy. Indicated in the figure both the fundamental Rayleigh (green ellipse) and Love (light blue ellipse) wave energy are indicated. The Rayleigh wave is visible with a high ellipticity signal. The back azimuth obtained from the Rayleigh wave is similar but offset to that obtained from body waves and is estimated to be about 120°. The Love wave has horizontal polarization as expected from a typical Love wave. In contrast to the Rayleigh wave, it has a low ellipticity, meaning the signal is linear. From both body waves and surface waves, we have a self-consistent set of polarization. To be consistent with the MQS catalogue, the preferred back azimuth is 101° (96°-112°).

2.5 Location of S1222a

Combining the distance and the back azimuth, the event can be located at 3.0°S, 171.9°E (Figure 3(c), Table 1). The uncertainty ellipse is indicated in the figure, dominated by the relatively wide uncertainty in backazimuth. The event appears to lie about 10°to the south to the farthest Eastern extent of Cerberus Fossae, by a considerably margin the most seismically active region on Mars (Giardini et al., 2020; Perrin et al., 2022; Rivas-Dorado et al., 2022; Zenhäusern et al., 2022; Stähler et al., 2022). The majority of located seismic events locate within this region (Ceylan et al., 2022) and a clear link between surface fault system and source mechanisms is suggested (Brinkman et al., 2021; Jacob et al., 2022). S1222a locates in a region closer to the North-South dichotomy (Smith et al., 2001). Unlike the Cerberus Fossae region, the epicenter of S1222a shows no evident tectonic features. In addition, no new crater of appropriate size has been detected in orbital images taken of the location error ellipse, thus far. Further investigation should be done with higher resolution imagery (e.g. MRO HiRISE).

2.6 Magnitude Evaluation

Following the methods described in (Böse et al., 2021), we obtained magnitudes for this event, which are summarized in Table 1. We assigned 3 types of magnitude depending on the frequency band and the method that we use to define the magnitude. The first, $M^{Ma}_{w,spec}$ was defined using the body wave spectrum and fitting this with omega square model. We obtained 4.7 ± 0.2 for the magnitude which is larger by 0.5 compared to the second largest event (S0976a,$M^{Ma}_{w,spec}$=4.2±0.3(Horleston et al., 2022)). This was viewed as the reference magnitude among the obtained magnitudes and was used to calculate the seismic moment. This magnitude is by far the largest of all the cataloged marsquakes and the seismic moment release of this single event is comparable to all other events in the marsquake catalog combined. The other two magnitudes were calculated from body wave amplitudes for P and S filtered at 2-6 seconds period. The body wave magnitude (m^{Ma}_b and m_bS^{Ma}) was obtained for P and S amplitude respectively and we obtained 5.3 and 5.8. The difference in the obtained magnitude can be explained by the high corner frequency compared to other marsquakes (Stähler et al., 2022).

2.7 Spectral analysis

S1222a shows one of the richest frequency contents ever seen within marsquakes with a significantly wider frequency band that range from 1/30 Hz to 35 Hz, compared to previously detected events. Both P and S arrivals have broadband energy covering frequencies as low as ∼0.02 Hz up to ∼35 Hz (Figure 1(c), Figure 2). The noise starts

to increase below ∼0.4 Hz and becomes dominant at ∼0.01 Hz. The S wave extends over a wider frequency band, covering both lower and higher frequencies compared to the P wave. At high frequencies above 1 Hz, the P and S waves have similar spectral shapes that almost overlap with each other.

When we compare spectra from the vertical and horizontal components, we see clear enhancement for horizontal components (Figure 1(c)). While the spectrum of the vertical component decays rapidly with frequency, the horizontal components show almost flat or slightly decaying spectra. This is a typical characteristic observed for VF type events. Such a feature was not observed for other BB type events. At frequencies higher than 1 Hz, we see a characteristic peak centered around 2.4 Hz. The resonance at 2.4 Hz is widely known and was reported in previous studies (van Driel et al., 2021; Dahmen et al., 2021; Hobiger et al., 2021). The high corner frequency of the event is unusual for other relatively large marsquakes, specifically those observed in Cerberus Fossae (Stähler et al., 2022), and suggests that the event occurs outside this fault system, which is consistent with the location we obtained.

3 Discussion

3.1 Possible Aftershock

About 34 hours after S1222a, a small VF event was detected (S1223a). While this was a much weaker event compared to S1222a (M_W^{Ma}=2.9), the event was carefully examined given the possibility of it being an aftershock of S1222a. S1223a clearly lacks long period energy compared to S1222a, thus it is cataloged as a VF event and not a BB event. This is unlikely for an aftershock but this might be due to the large difference in the magnitudes of the two events. Due to strong environmental noise injection at the time of S1223a, the time differences between the P and S arrivals were constrained through comodulation from weather-sensitive lander resonances (Charalambous et al., 2021) and indicate similar time delays for both events (3 minutes 20 seconds and 3 minutes 34 seconds). As is often the case for VF events, no polarization can be assigned.

3.2 Additional Multi-orbit Phases

S1222a is so large that beyond the multi-orbit R3 phase arrival there are hints for further phase arrivals, which are labelled in Figure1 and Table 1 as x4 and x5. The pre-landing expectation was that locations could be made using any combination of body phases and surface waves. In the pre-launch blind test (Clinton et al., 2017; van Driel et al., 2019), source locations were tested using body waves and R1/R2/R3. Further multi-orbit phases were not considered or its utilisation was not tested (Panning et al., 2015; Böse et al., 2017). However, for S1222a, we were able to identify some increases in energy on the vertical component at around the expected time windows for R4 and R5. The signal to noise ratio is low and we were not able to see any clear phase of dispersion in the data, leaving some uncertainties in their identification as R4 and R5. Thus, we included these signals in the catalog as x4 and x5, using the indicator x, which MQS uses for unknown phases. While we would like to leave future studies to confirm this, we believe that these arrivals are possible candidates for R4 and R5.

4 Conclusion

We reported in this study the general characteristics of S1222a, the magnitude 4.7 marsquake located 37°distance from the SEIS seismometer, which is by far the largest event detected during the InSight mission to date. Both body waves and a rich suite of surface waves can be identified, including both fundamental and first overtone Rayleigh and Love waves, and multi orbit Rayleigh waves. As recorded at InSight, the event includes energy ranging from below 1/30 Hz up to 35Hz. In the context of the marsquake

catalog event types, the low frequency component (<2.4Hz) resembles broadband type events whereas the higher frequency component is characteristic of very high frequency events. Such an event may provide us with a clue to understand the different types of marsquakes and their origins. The event is located close to the the North/South dichotomy of Mars and outside the well-known Cerberus Fossae region where many of the major seismic events are located. These features require further investigation and the event will serve as an unique example to uncover the mysteries of Martian seismicity.

Acknowledgments

We acknowledge NASA, CNES, partner agencies and institutions (UKSA, SSO, DLR, JPL, IPGP-CNRS, ETHZ, ICL, MPS-MPG), and the operators of JPL, SISMOC, MSDS, IRISDMC and PDS for providing SEED SEIS data. Marsquake Service (MQS) operations at ETH are supported by ETH Research grant ETH-06 17-02. ETH authors recognise support from the ETH+ funding scheme (ETH+02 19-1: "Planet Mars"). French co-authors acknowledge support of the French Space Agency CNES and Agence Nationale de la Recherche, ANR (ANR-19-CE31-0008-08). TK, MP, PL, GS acknowledge support of IdEx Université Paris Cité ANR-18-IDEX-0001. A.H. is funded by the UK Space Agency under grant numbers ST/R002096/1 and ST/W002523/1. This research was carried out in part at the Jet Propulsion Laboratory, California Institute of Technology, under a contract with the National Aeronautics and Space Administration (80NM0018D0004). This paper is InSight Contribution Number 285.

Open Research

All raw waveform data is available through the InSight Mars SEIS Data Service @ IPGP, IRIS-DMC and NASA PDS. (InSight Mars SEIS Data Service, 2019).

Table 1: General information of S1222a and Phase Picks from MQS

Event parameters	Event name S1222a
Origin time	
UTC	2022-05-04 23:23:07± 4.8s
LMST	03:54:39
Distance	37° (±1.6°)
Back-azimuth	101° (96°-112°)
Source Location	3.0 °S, 171.9 °E
M_w^{Ma} ($M_{w,spec}^{Ma}$)	4.7 ± 0.2
m_b^{Ma}	5.3
m_{bS}^{Ma}	5.8
Seismic Moment (N.m)	1.4×10^{16} ($7.0{\times}10^{15} \sim 2.8{\times}10^{16}$)
Peak amplitude (m/s)	
Vertical	1.3×10^{-5}
North	2.8×10^{-5}
East	2.8×10^{-5}
SNR (Seismic)	545194.7
Duration	∼633 min

Phase Arrivals	
Body waves	
P	23:27:45.8 (±0.5 s)
S	23:31:20.1 (±2 s)
y1	23:27:46.3 (±0.5 s)
y2	23:31:30.8 (±10 s)
Surface waves	
R1	
1/34 Hz	23:35:59.1 (±20 s)
1/28 Hz	23:35:58.3 (±20 s)
1/24 Hz	23:36:14.3 (-50.2 ∼ +42.0 s)
1/20 Hz	23:36:27.9 (±43.4 s)
1/17 Hz	23:36:48.2 (-40.7 ∼ +63.7 s)
1/14 Hz	23:38:01.4 (-47.5 ∼ +35.2 s)
1/12 Hz	23:38:08.2 (-73.2 ∼ +66.4 s)
R1-1	
1/14 Hz	23:33:33.0 (-36.1 ∼ +25.9 s)
1/12 Hz	23:33:59.4 (-19.8 ∼ +17.6 s)
1/10 Hz	23:34:09.1 (-19.4 ∼ +10.6 s)
1/8.4 Hz	23:34:12.6 (-21.6 ∼ +11.9 s)
1/7 Hz	23:34:23.2 (-11.9 ∼ +15.0 s)
1/6 Hz	23:34:23.6 (-11.9 ∼ +10.1 s)
1/5 Hz	23:34:24.9 (-14.0 ∼ +15.4 s)
1/4.2 Hz	23:34:25.8 (-10 ∼ +11.21 s)
1/3.5 Hz	23:34:26.0 (-8.8 ∼ +9.4 s)
R2	
1/34 Hz	01:14:05 (-70.5 ∼ +66.6 s)
1/28 Hz	01:13:49.4 (-62.7 ∼ +43.1 s)
R3	
1/34 Hz	01:38:57.5 (-340.8 ∼ +78.3 s)
1/28 Hz	01:39:17.1 (-141 ∼ +66.6 s)
G1	
1/48 Hz	23:33:38.2 (-84.7 ∼ +103.0 s)
1/40 Hz	23:33:38.2 (-84.7 ∼ +53.2 s)
1/34 Hz	23:33:38.2 (-70.0 ∼ +104.7 s)
1/28 Hz	23:34:03.1 (-131.3 ∼ +156.2 s)
1/24 Hz	23:34:04.9 (-51.0 ∼ +31.3 s)
1/20 Hz	23:34:23.0 (-70.8 ∼ +52.7 s)
1/17 Hz	23:34:31.2 (-32.9 ∼ +29.6 s)
1/14 Hz	23:34:36.1 (-39.5 ∼ +42.8 s)
1/12 Hz	23:34:20.3 (-26.7 ∼ +31.3 s)
G1-1	
1/12 Hz	23:33:33.9 (-16.8 ∼ +12.2 s)
1/10 Hz	23:33:40.0 (-19.0 ∼ +18.2 s)
1/8.4 Hz	23:33:41.4 (-17.4 ∼ +31.0 s)
1/7 Hz	23:33:48.4 (-14.7 ∼ +28.9 s)
1/6 Hz	23:34:17.8 (-11.0 ∼ +13.5 s)
1/5 Hz	23:34:19.8 (14.6 ∼ +31.9 s)
x4	03:16:43.3 (±60 s)
x5	03:42:00.6 (±60 s)

manuscript submitted to *Geophysical Research Letters*

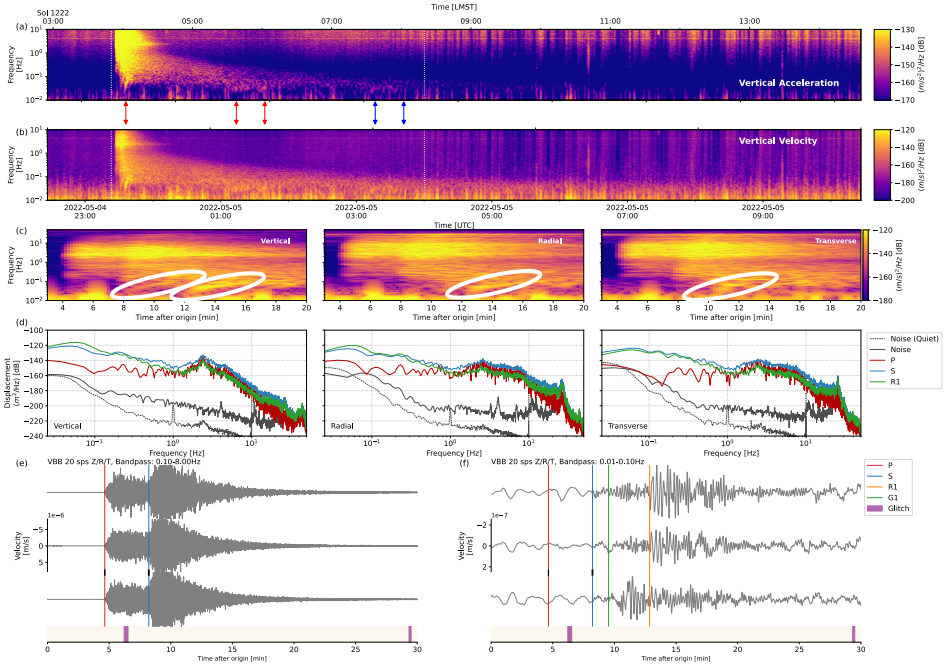

Figure 1: Event summary for S1222a. (a) 12 hour spectrogram in acceleration on the long period signal of the event. 20Hz deglichted data was used for the plot. Time window of 200 second with 90% overlap was used. The 3 red arrows below indicate R1/2/3 arrivals from the MQS catalog and the 2 blue arrows correspond to the x4 and x5 arrivals. The white dotted line is the origin time and the event end time from the catalog. (b) 12 hour spectrogram in velocity including the high frequency energy. The same time window and overlap as (a) was used. (c) 3 axes velocity spectrogram zoomed in to the event and expanded to the full frequency band width. 100 Hz deglitched data were used for the plot. Time window of 100 seconds and overlap of 90% were used. The signal (d) Spectra of P, S and R1 energy of the event compared with pre-event noise and the noise level of a quiet period during the mission (noise curve of Sol 0235 were taken). To calculate P and S spectra, spectral time windows in the MQS catalog were used. For the noise, we also referred to the noise window in the catalog. For the noise level of the quiet season, we took noise window of marsquake S0235b. (e) Seismograms filtered between 0.1-0.8 Hz. The red and the blue lines refer to P and S arrival times identified by MQS. Glitches identified by MQS are indicated in purple in the bottom.(f) Seismograms filtered between 0.01-0.1 Hz. The red and blue lines refer to P and S arrival times identified by MQS. Arrival times of fundamental Rayleigh and Love waves are shown in orange and green. For the surface waves the earliest arrival of all the frequency bands are shown in the figure. For (c)-(f), the signal were rotated to vertical, radial and transverse component using the back-azimuth we obtained (Table1)

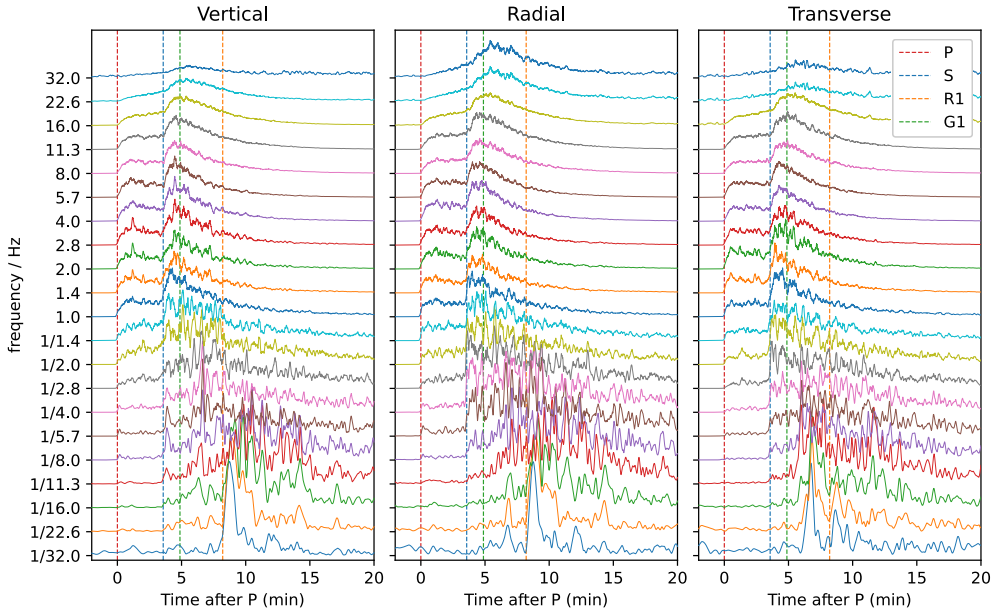

Figure 2: Filterbanks of S1222a. To create the filterbanks, both 20 Hz and 100 Hz data were used. Frequencies above 10 Hz used 100 Hz channels and were deglitched using the seisdeglitch tool (https://pss-gitlab.math.univ-paris-diderot.fr/data-processing-wg/seisglitch). The low frequencies below 10 Hz used 20 Hz continuous VBB channels and were deglitched with the method developed in UCLA (see Scholz et al. (2020) for further details) which achieves more efficient deglitching but is not applicable to 100 Hz data. The deglitching was tailored specifically for the event and was more efficient in removing glitches within the P and S code. Each trace shows the filtered envelope smoothed with 10 second time window. Each trace is bandpass-filtered at the frequencies shown in the y-axis. The filters are half an octave wide on each side. Body (P and S) and surface wave (Rayleigh and Love) arrivals are indicated with vertical dashed lines.

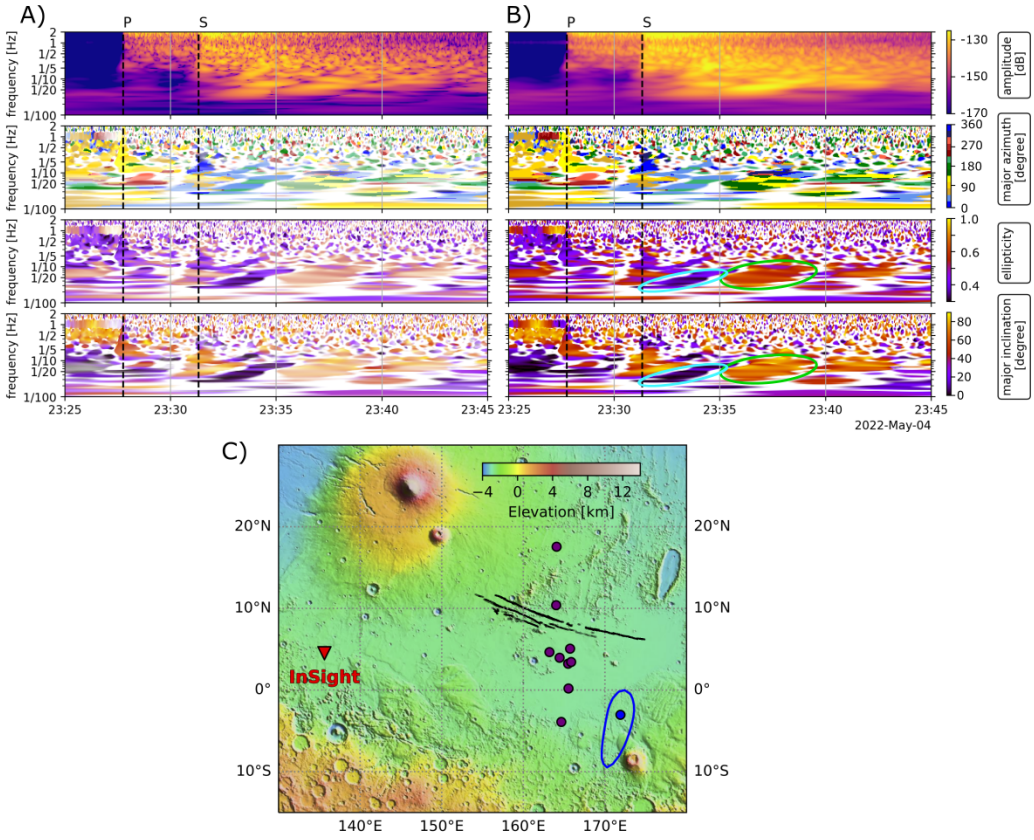

Figure 3: Polarisation and location of S1222a. (a) Data filtered to enhance linear, polarised signals. (b) Data filtered to enhance only polarised data, no linearity filter. Love and Rayleigh waves with overtones are visible after the S wave pick. For both (a) and (b): Back Azimuth of S1222a obtained from eigenvector methods (Zenhäusern et al., 2022) using de-glitched data; time-frequency depiction of (top row) amplitude, (second row) azimuth, (third row) ellipticity, and (bottom row) inclination. (c) Shown are quality A event locations (purple dots) and the InSight location (red triangle). The location of S1222a is marked by the blue uncertainty ellipse with a blue dot to show the preferred location. The Cerberus Fossae graben are marked with black lines. Updated from (Zenhäusern et al., 2022). The map background uses Mars Orbiter Laser Altimeter elevation data (Smith et al., 2001).

References

Banerdt, W. B., Smrekar, S. E., Banfield, D., Giardini, D., Golombek, M., Johnson, C. L., ... Wieczorek, M. (2020). Initial results from the InSight mission on Mars. *Nat. Geosci.*, *13*(3), 183–189. doi: 10.1038/s41561-020-0544-y

Banfield, D., Rodriguez-Manfredi, J. A., Russell, C. T., Rowe, K. M., Leneman, D., Lai, H. R., ... Banerdt, W. B. (2019). InSight Auxiliary Payload Sensor Suite (APSS). *Space Sci. Rev.*, *215*(1), 4. doi: 10.1007/s11214-018-0570-x

Banfield, D., Spiga, A., Newman, C., Forget, F., Lemmon, M., Lorenz, R., ... Banerdt, W. B. (2020). The atmosphere of Mars as observed by InSight. *Nat. Geosci.*, *13*(3), 190–198. doi: 10.1038/s41561-020-0534-0

Böse, M., Clinton, J. F., Ceylan, S., Euchner, F., van Driel, M., Khan, A., ... Banerdt, W. B. (2017). A probabilistic framework for single-station location of seismicity on Earth and Mars. *Phys. Earth Planet. Inter*, *262*, 48–65. doi: https://doi.org/10.1016/j.pepi.2016.11.003

Böse, M., Stähler, S. C., Deichmann, N., Giardini, D., Clinton, J., Lognonné, P., ... Banerdt, W. B. (2021, Jun 22). Magnitude scales for marsquakes calibrated from insight data. *Bull. Seismol. Soc. Am.*. doi: 10.1785/0120210045

Brinkman, N., Stähler, S. C., Giardini, D., Schmelzbach, C., Khan, A., Jacob, A., ... Banerdt, W. B. (2021). First focal mechanisms of marsquakes. *J. Geophys. Res.: Planets*, *126*(4), e2020JE006546. doi: https://doi.org/10.1029/2020JE006546

Ceylan, S., Clinton, J. F., Giardini, D., Böse, M., Charalambous, C., van Driel, M., ... Perrin, C. (2021). Companion guide to the marsquake catalog from InSight, Sols 0–478: Data content and non-seismic events. *Phys. Earth Planet. Inter.*, *310*, 106597. doi: https://doi.org/10.1016/j.pepi.2020.106597

Ceylan, S., Clinton, J. F., Giardini, D., Stähler, S. C., Horleston, A., Kawamura, T., ... Banerdt, W. B. (2022). The marsquake catalogue from insight, sols 0–1011. *Phys. Earth Planet. Inter.*, 106943. doi: 10.1016/j.pepi.2022.106943

Charalambous, C., Stott, A. E., Pike, W. T., McClean, J. B., Warren, T., Spiga, A., ... Banerdt, W. B. (2021). A comodulation analysis of atmospheric energy injection into the ground motion at insight, mars. *J. Geophys. Res.: Planets*, *126*(4), e2020JE006538. doi: https://doi.org/10.1029/2020JE006538

Clinton, J. F., Ceylan, S., van Driel, M., Giardini, D., Stähler, S. C., Böse, M., ... Stott, A. E. (2021). The marsquake catalogue from insight, sols 0–478. *Phys. Earth Planet. Inter.*, *310*, 106595. doi: https://doi.org/10.1016/j.pepi.2020.106595

Clinton, J. F., Giardini, D., Lognonné, P., Banerdt, B., van Driel, M., Drilleau, M., ... Spiga, A. (2017, 07). Preparing for InSight: An Invitation to Participate in a Blind Test for Martian Seismicity. *Seismological Research Letters*, *88*(5), 1290-1302. Retrieved from `https://doi.org/10.1785/0220170094` doi: 10.1785/0220170094

Dahmen, N. L., Zenhäusern, G., Clinton, J. F., Giardini, D., Stähler, S. C., Ceylan, S., ... Banerdt, W. B. (2021, 10). Resonances and Lander Modes Observed by InSight on Mars (1–9 Hz). *Bull. Seismol. Soc. Am.*, *111*(6), 2924-2950. doi: 10.1785/0120210056

Drilleau, M., Samuel, H., Garcia, R. F., Rivoldini, A., Perrin, C., Michaut, C., ... Banerdt, W. B. (2022). Marsquake locations and 1-d seismic models for mars from insight data. *Journal of Geophysical Research: Planets*, *127*(9), e2021JE007067. Retrieved from `https://agupubs.onlinelibrary.wiley.com/doi/abs/10.1029/2021JE007067` (e2021JE007067 2021JE007067) doi: https://doi.org/10.1029/2021JE007067

Drilleau, M., Samuel, H., Rivoldini, A., Panning, M., & Lognonné, P. (2021, 03). Bayesian inversion of the Martian structure using geodynamic constraints. *Geophys. J. Int.*, *226*(3), 1615-1644. doi: 10.1093/gji/ggab105

Garcia, R. F., Daubar, I. J., Beucler, É., Posiolova, L. V., Collins, G. S., Lognonné,

P., ... Banerdt, W. B. (2022, Sep 19). Newly formed craters on mars located using seismic and acoustic wave data from insight. *Nature Geoscience*. Retrieved from https://doi.org/10.1038/s41561-022-01014-0 doi: 10.1038/s41561-022-01014-0

Giardini, D., Lognonné, P., Banerdt, W. B., Pike, W. T., Christensen, U., Ceylan, S., ... Yana, C. (2020). The Seismicity of Mars. *Nat. Geosci.*. doi: 10.1038/s41561-020-0539-8

Hobiger, M., Hallo, M., Schmelzbach, C., Stähler, S. C., Fäh, D., Giardini, D., ... Banerdt, W. B. (2021, Nov 23). The shallow structure of mars at the insight landing site from inversion of ambient vibrations. *Nature Communications*, *12*(1), 6756. doi: 10.1038/s41467-021-26957-7

Horleston, A., Clinton, J., Ceylan, S., Giardini, D., Charalambous, C., Irving, J., ... Banerdt, W. (2022). The far side of Mars: two distant marsquakes detected by InSight. *The Seismic Record*. doi: 10.1785/0320220007

InSight Mars SEIS Data Service. (2019). *Seis raw data, insight mission.* IPGP, JPL, CNES, ETHZ, ICL, MPS, ISAE-Supaero, LPG, MFSC. Retrieved from https://datacenter.ipgp.fr/networks/detail/XB_2016/ doi: 10.18715/SEIS.INSIGHT.XB_2016

Jacob, A., Plasman, M., Perrin, C., Fuji, N., Lognonné, P., Xu, Z., ... Banerdt, W. (2022). Seismic sources of insight marsquakes and seismotectonic context of elysium planitia, mars. *Tectonophysics*, *837*, 229434. Retrieved from https://www.sciencedirect.com/science/article/pii/S0040195122002281 doi: https://doi.org/10.1016/j.tecto.2022.229434

Johnson, C. L., Mittelholz, A., Langlais, B., Russell, C. T., Ansan, V., Banfield, D., ... Banerdt, W. B. (2020, 3). Crustal and time-varying magnetic fields at the InSight landing site on Mars. *Nature Geoscience*, *13*(3), 199–204. doi: 10.1038/s41561-020-0537-x

Karakostas, F., Schmerr, N., Maguire, R., Huang, Q., Kim, D., Lekic, V., ... Banerdt, B. (2021, 10). Scattering Attenuation of the Martian Interior through Coda-Wave Analysis. *Bulletin of the Seismological Society of America*, *111*(6), 3035-3054. Retrieved from https://doi.org/10.1785/0120210253 doi: 10.1785/0120210253

Khan, A., Ceylan, S., van Driel, M., Giardini, D., Lognonné, P., Samuel, H., ... Banerdt, W. B. (2021). Upper mantle structure of Mars from InSight seismic data. *Science*, *373*(6553), 434–438. doi: 10.1126/science.abf2966

Kim, D., Banerdt, W. B., Ceylan, S., Giardini, D., Lekić, V., Lognonné, P., ... Panning, M. P. (2022). Surface waves and crustal structure on mars. *Science*, *378*(6618), 417-421. Retrieved from https://www.science.org/doi/abs/10.1126/science.abq7157 doi: 10.1126/science.abq7157

Kim, D., Davis, P., Lekić, V., Maguire, R., Compaire, N., Schimmel, M., ... Banerdt, W. B. (2021, 10). Potential Pitfalls in the Analysis and Structural Interpretation of Seismic Data from the Mars InSight Mission. *Bull. Seismol. Soc. Am.*, *111*(6), 2982-3002. doi: 10.1785/0120210123

Kim, D., Lekić, V., Irving, J. C. E., Schmerr, N., Knapmeyer-Endrun, B., Joshi, R., ... Banerdt, W. B. (2021). Improving constraints on planetary interiors with pps receiver functions. *Journal of Geophysical Research: Planets*, *126*(11), e2021JE006983. Retrieved from https://agupubs.onlinelibrary.wiley.com/doi/abs/10.1029/2021JE006983 (e2021JE006983 2021JE006983) doi: https://doi.org/10.1029/2021JE006983

Knapmeyer-Endrun, B., Panning, M. P., Bissig, F., Joshi, R., Khan, A., Kim, D., ... Banerdt, W. B. (2021). Thickness and structure of the martian crust from insight seismic data. *Science*, *373*(6553), 438–443. doi: 10.1126/science.abf8966

Lognonné, P., Banerdt, W., Giardini, D., Pike, W., Christensen, U., Laudet, P., ... Wookey, J. (2019). SEIS: Insight's Seismic Experiment for Internal Structure of

Mars. *Space Sci. Rev.*, *215*(1), 12. doi: 10.1007/s11214-018-0574-6

Lognonné, P., Banerdt, W., Pike, W., Giardini, D., Christensen, U., Garcia, R., ... Zweifel, P. (2020). Constraints on the shallow elastic and anelastic structure of Mars from InSight seismic data. *Nat. Geosci.*. doi: 10.1038/s41561-020-0536-y

Menina, S., Margerin, L., Kawamura, T., Lognonné, P., Marti, J., Drilleau, M., ... Banerdt, W. B. (2021, 11). Energy Envelope and Attenuation Characteristics of High-Frequency (HF) and Very-High-Frequency (VF) Martian Events. *Bulletin of the Seismological Society of America*, *111*(6), 3016-3034. Retrieved from `https://doi.org/10.1785/0120210127` doi: 10.1785/0120210127

Panning, M. P., Beucler, E., Drilleau, M., Mocquet, A., Lognonné, P., & Banerdt, W. B. (2015). Verifying single-station seismic approaches using Earth-based data: Preparation for data return from the InSight mission to Mars. *Icarus*, *248*, 230 - 242. doi: 10.1016/j.icarus.2014.10.035

Perrin, C., Jacob, A., Lucas, A., Myhill, R., Hauber, E., Batov, A., ... Fuji, N. (2022). Geometry and segmentation of cerberus fossae, mars: Implications for marsquake properties. *J. Geophys. Res.: Planets*, *127*(1), e2021JE007118. doi: https://doi.org/10.1029/2021JE007118

Posiolova, L. V., Lognonné, P., Banerdt, W. B., Clinton, J., Collins, G. S., Kawamura, T., ... Zenhäusern, G. (2022). Largest recent impact craters on mars: Orbital imaging and surface seismic co-investigation. *Science*, *378*(6618), 412-417. Retrieved from `https://www.science.org/doi/abs/10.1126/science.abq7704` doi: 10.1126/science.abq7704

Rivas-Dorado, S., Ruíz, J., & Romeo, I. (2022). Giant dikes and dike-induced seismicity in a weak crust underneath cerberus fossae, mars. *Earth and Planetary Science Letters*, *594*, 117692. Retrieved from `https://www.sciencedirect.com/science/article/pii/S0012821X22003284` doi: https://doi.org/10.1016/j.epsl.2022.117692

Scholz, J.-R., Widmer-Schnidrig, R., Davis, P., Lognonné, P., Pinot, B., Garcia, R. F., ... Banerdt, W. B. (2020). Detection, Analysis, and Removal of Glitches From InSight's Seismic Data From Mars. *Earth and Space Science*, *7*(11), e2020EA001317. doi: https://doi.org/10.1029/2020EA001317

Smith, D. E., Zuber, M. T., Frey, H. V., Garvin, J. B., Head, J. W., Muhleman, D. O., ... Sun, X. (2001). Mars orbiter laser altimeter: Experiment summary after the first year of global mapping of mars. *J. Geophys. Res.: Planets*, *106*(E10), 23689-23722. doi: https://doi.org/10.1029/2000JE001364

Stähler, S. C., Khan, A., Banerdt, W. B., Lognonné, P., Giardini, D., Ceylan, S., ... Smrekar, S. E. (2021). Seismic detection of the martian core. *Science*, *373*(6553), 443–448. doi: 10.1126/science.abi7730

Stähler, S. C., Mittelholz, A., Perrin, C., Kawamura, T., Kim, D., Knapmeyer, M., ... Banerdt, W. B. (2022, Oct 27). Tectonics of cerberus fossae unveiled by marsquakes. *Nature Astronomy*. Retrieved from `https://doi.org/10.1038/s41550-022-01803-y` doi: 10.1038/s41550-022-01803-y

Stutzmann, E., Schimmel, M., Lognonné, P. H., Horleston, A. C., Ceylan, S., van Driel, M., ... et al. (2020). Polarized ambient noise on mars. *Earth and Space Science Open Archive*, 41. doi: 10.1002/essoar.10503376.1

van Driel, M., Ceylan, S., Clinton, J. F., Giardini, D., Alemany, H., Allam, A., ... Zheng, Y. (2019). Preparing for InSight: Evaluation of the blind test for martian seismicity. *Seismol. Res. Lett.*, *90*(4). doi: https://doi.org/10.1785/0220180379

van Driel, M., Ceylan, S., Clinton, J. F., Giardini, D., Horleston, A., Margerin, L., ... Banerdt, W. B. (2021). High-frequency seismic events on Mars observed by InSight. *J. Geophys. Res.: Planets*, *126*(2), e2020JE006670. doi: https://doi.org/10.1029/2020JE006670

Zenhäusern, G., Stähler, S. C., Clinton, J. F., Giardini, D., Ceylan, S., & Garcia, R. F. (2022). Low frequency marsquakes and where to find them: Back azimuth

503 determination using a polarization analysis approach. *Bull. Seismol. Soc. Am.*,
504 1–19. doi: 10.1785/0120220019
505 Zweifel, P., Mance, D., ten Pierick, J., Giardini, D., Schmelzbach, C., Haag, T., ...
506 Banerdt, W. B. (2021, 10). Seismic High-Resolution Acquisition Electronics for
507 the NASA InSight Mission on Mars. *Bull. Seismol. Soc. Am.*, *111*(6), 2909-2923.
508 doi: 10.1785/0120210071